

# Combined Upper Limits on MSSM Higgs-Boson Production in association with a $b$ -quark with up to $7.3 \text{ fb}^{-1}$ of Data at DØ

The DØ Collaboration  
URL <http://www-d0.fnal.gov>

Results are presented on the search for a neutral MSSM Higgs boson produced in association with one or more  $b$ -quarks, combining the  $bh \rightarrow b\tau\tau$  and  $bh \rightarrow b\bar{b}\bar{b}$  final states, using an integrated luminosity of  $7.3 \text{ fb}^{-1}$  and  $5.2 \text{ fb}^{-1}$  respectively, collected at the DØ experiment. Data were collected in  $p\bar{p}$  collisions at a center of mass energy of 1.96 TeV during RunII of the Tevatron. Limits at the 95% confidence level are set on the production cross section of a Higgs boson in association with one or more  $b$ -quarks,  $\sigma(gb \rightarrow hb(b))$ , for Higgs masses,  $90 < M_A < 300$ , assuming a narrow Higgs width respect to the experimental resolution and the sum rule  $\text{BR}(h \rightarrow \tau\tau) + \text{BR}(h \rightarrow b\bar{b}) = 1$ , for  $\text{BR}(h \rightarrow \tau\tau) = 0.06, 0.1$  and  $0.14$ . Further interpretation, including width effects, is made in the  $\tan \beta$ - $M_A$  plane for four different benchmark scenarios within the framework of the MSSM.

*Preliminary Results*

## I. INTRODUCTION

Supersymmetry (SUSY) as an extension to the Standard Model (SM) provides a natural solution to the hierarchy problem as well as potentially providing a dark matter candidate and GUT-scale unification. In its simplest form the Minimal Supersymmetry Standard Model [1] (MSSM) requires the introduction of two Higgs doublet fields, predicting the existence of five physical Higgs bosons after symmetry breaking. Three of these are neutral ( $h$ ,  $H$ , and  $A$ ) and two are charged  $H^\pm$ . The ratio of the vacuum expectation values of the two doublets is denoted by  $\tan \beta$ . At leading order the Higgs sector can be described by two parameters chosen here to be  $M_A$  (the mass of the  $A$ ) and  $\tan \beta$ . The couplings of the  $A$  to the charged leptons and the down-type quarks are enhanced by a factor of  $\tan \beta$ , while the coupling to neutrinos and up-type quarks are suppressed by a similar factor. At large values of  $\tan \beta$  two of the three neutral bosons have approximately the same mass and couplings thus are effectively degenerate. This contributes an additional factor of two enhancement in the cross section. Thus the overall enhancement at leading-order scales approximately as  $2 \times \tan^2 \beta$ . For low  $M_A$ , and high  $\tan \beta$  the Tevatron can set strong limits within a number of benchmark scenarios in the MSSM that complement the searches carried out by the LEP experiments [2].

## II. ANALYSIS SUMMARY

The  $D\bar{O}$  detector is described in detail elsewhere [3]. The searches combined in this analysis are described in detail in [4, 5]. Two semi-exclusive searches looking for Higgs production in association with a  $b$ -quark are combined:  $bh \rightarrow b\tau\tau$  ( $\tau_\mu\tau_{\text{had}}$ ) and  $bh \rightarrow bb\bar{b}$  using respectively,  $7.3 \text{ fb}^{-1}$  and  $5.2 \text{ fb}^{-1}$  of integrated luminosity collected during Run II at the Tevatron. Though not included in this combination, earlier searches at  $D\bar{O}$  can be found in [6–10, 12? ] . Results of similar searches from CDF in Run II at the Tevatron are found in [13–15]. Recent results from the CMS collaboration can be found in [16].

### A. Object Identification

Muons are identified by matching charged tracks in the central tracking detectors with hits in the muon detectors. Muon candidates are also required to be isolated in both the central tracking detectors and in the calorimeter. The hadronic decays of the  $\tau$  are split into three categories:  $\tau$ -types 1 and 2 are 1-prong candidates with energy either only in the hadron calorimeter ( $\pi^\pm$  like) or in both the electromagnetic and hadron calorimeters ( $\rho^\pm$  like) respectively;  $\tau$ -type 3 is a 3-prong candidate with an invariant mass below 1.7 GeV and matching energy deposits in the calorimeters. A neural network ( $\text{NN}_\tau$ ) is trained for each type to separate hadronic tau decays from jets using Monte-Carlo (MC)  $Z \rightarrow \tau\tau$  as the signal and multi-jet events taken from data as the background. An additional NN is trained on electron MC events and is employed to reduce backgrounds from electrons faking type 2 taus. A mid-point cone algorithm is used to reconstruct hadronic jets from energy deposits in the calorimeter [17]. Jet reconstruction and energy scale determination are described in detail in [18].  $b$ -jet candidates must pass a set of quality criteria, and must have two or more charged tracks within a cone about the jet axis of radius:  $\Delta R = \sqrt{(\Delta\eta)^2 + (\Delta\phi)^2} < 0.5$ .  $b$ -jets are then identified using a neural network ( $\text{NN}_{\text{btag}}$ ) algorithm which takes as inputs lifetime information derived from track impact parameters and secondary vertices [19].

### B. Signal, Backgrounds and Event Selection

The signal acceptance is estimated using simulated  $gb \rightarrow hb(b)$  events generated, in the 5-flavor scheme, with the leading-order (LO) Monte Carlo generator PYTHIA [20]. Corrections for next-to-leading order (NLO) effects on the Higgs production kinematics are computed using MCFM [21] and applied as weights as a function of  $p_T$  and  $\eta$  of the spectator  $b$ -jet. Kinematic cuts,  $p_T > 12 \text{ GeV}$ ,  $|\eta| < 5.0$ , are applied to the leading spectator  $b$ -quark. TAUOLA [22] is used to simulate the final state tau decays. Detector response is modeled using GEANT [24] based simulations and additional weights are applied to correct for the trigger efficiency and differences between the simulation and detector performance determined from control samples. The effect of additional  $p\bar{p}$  interactions is modeled by overlaying data events selected with random triggers on the Monte Carlo events. With the exception of diboson production, generated using PYTHIA, standard model backgrounds have been generated with ALPGEN matched to PYTHIA for showering and hadronization. The normalization of the di-boson and  $t\bar{t}$  samples is made to next-to-LO (NLO) while the  $Z/\gamma^*$  samples are normalised to next-to-NLO (NNLO).

1.  $bh \rightarrow b\tau\tau$ 

Data events are collected online using an inclusive trigger selection comprising a mix of single muon, jet, tau, muon plus jet, and muon plus tau triggers. The efficiency of this selection with respect to the single muon trigger alone is estimated using a sample of  $Z \rightarrow \tau_\mu \tau_{\text{had}}$  events and found to lie between 80% and 95% dependent on the event kinematics and the type of hadronic tau decay. Events are required to contain one isolated muon with a matching central track, satisfying  $p_T > 15$  GeV and  $|\eta_{\text{det}}| < 1.6$  [25] and events with more than one muon are rejected to suppress backgrounds from  $Z \rightarrow \mu\mu$ . Hadronic- $\tau$  candidates are required to be isolated, with  $p_T > 10$  GeV and  $|\eta_\tau| < 2.5$  and selected with a cut on the output of the  $\text{NN}_\tau$  discriminant with an efficiency of around 65% whilst rejecting approximately 99% of hadronic jets. Events must have at least one good  $b$ -tagged jet isolated from the muon and tau with  $p_T > 15$  GeV,  $|\eta| < 2.5$ , and  $|\eta_{\text{det}}| < 2.5$ . A cut is placed on the  $\text{NN}_{\text{btag}}$  with an efficiency of around 65% for  $b$ -quark jets and a 5% fake rate for light quark and gluon jets. Additional rejection of multi-jet and top pair production backgrounds is achieved using a multivariate discriminant,  $\mathcal{D}_{\text{MJ}}$ , and a neural network,  $\mathcal{D}_{t\bar{t}}$ , respectively, both making use of kinematic variables. The distribution of a likelihood discriminant,  $\mathcal{D}_f$ , is used as input to the statistical analysis. This is constructed from the various multivariate discriminants,  $\mathcal{D}_{\text{MJ}}$ ,  $\mathcal{D}_{t\bar{t}}$ ,  $\text{NN}_{\text{btag}}$  and a further variable relating to the decay kinematics  $M_{\text{hat}}$ . The distribution of  $\mathcal{D}_f$  summed over all tau types, though the three types are handled separately in the statistical treatment, is shown in Figure 1.

Dominant backgrounds arise from multi-jet production, top pair production, and  $Z \rightarrow \tau\tau$  produced with heavy flavor jets. Additional backgrounds making small contributions come from processes such as  $Z \rightarrow \tau\tau$  + light jets,  $Z \rightarrow ll$ ,  $W$ +jets, single top-quark production and diboson production. The distribution of the background from  $W$ +jets is modeled from simulation but the overall yield is normalised to data using a control sample. The multi-jet background is estimated from data using inverted lepton and tau identification cuts and no  $b$ -tagging to select a multi-jet rich background sample. The yields of the remaining backgrounds are estimated using the acceptance as determined from simulation, tuned using control samples, multiplied by the theoretical cross sections.

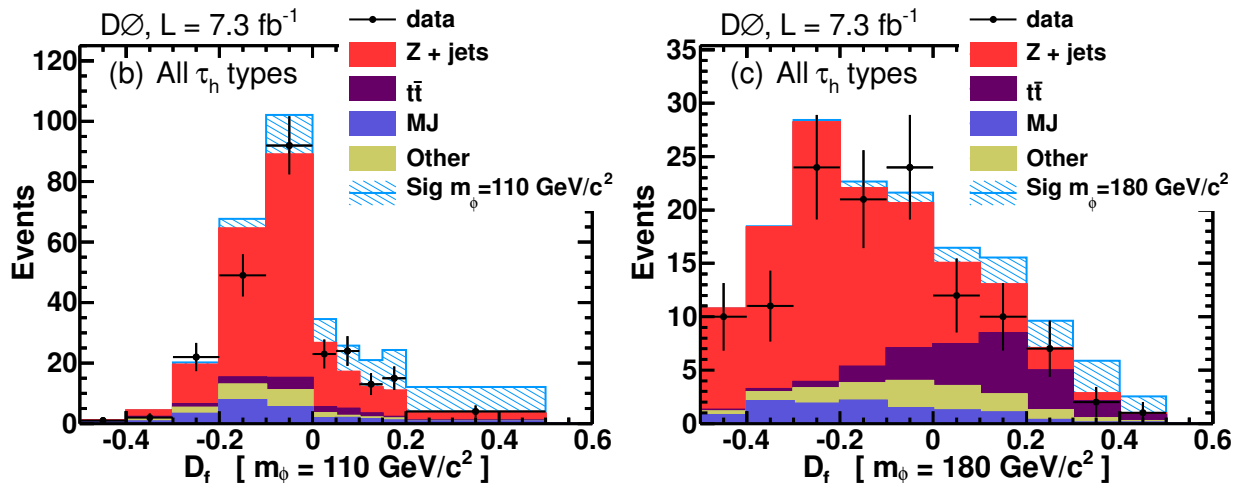


FIG. 1: Input distributions for the  $bh \rightarrow b\tau\tau$  channels. The final likelihood discriminant distribution summed over all tau types is shown for a Higgs mass of 110 GeV in the left panel and 180 GeV in the right panel. The stacked solid histograms show the various contributions from backgrounds, the hatched histogram shows the possible signal contribution and the points show the data.

2.  $bh \rightarrow b\bar{b}\bar{b}$ 

Dedicated triggers designed to select events with at least three jets are used in this analysis. These are approximately 60% efficient for signal with  $m_A = 150$  GeV when measured with respect to events with 3 or 4 reconstructed jets. At least three jets within the fiducial region ( $p_T > 20$  GeV,  $|\eta| < 2.5$ ) are required to pass tight  $\text{NN-}b$ -tagging cuts. The per  $b$ -jet tagging efficiency is around 50% with a light-jet fake rate at the level of 0.5-1.5%. Additionally, the two leading jets must have  $p_T > 25$  GeV. Signal sensitivity is further enhanced by breaking the sample into two channels containing exactly 3 or 4 fiducial jets in the final state. A likelihood technique using a set of kinematic variables is employed to further enhance the selection of signal over background. Two separate likelihoods are used:

one for the mass region  $90 \leq M_A < 140$  GeV and the other for  $140 \leq M_A < 260$  GeV. Heavy flavor multi-jet backgrounds dominate and are estimated using a data driven method by applying a 2-D-transformation (in  $M_{b\bar{b}}$  and  $\mathcal{D}$  the value of the likelihood discriminant) to a data sample containing  $\geq 2$   $b$ -tagged jets, derived from the ratio of MC events containing  $\geq 3$   $b$ -tagged jets to those containing  $\geq 2$   $b$ -tagged jets. The use of a ratio in this manner significantly reduces the sensitivity of the background model to the underlying kinematics of the simulated events and the modelling of the geometric acceptance of the detector. The binned invariant mass distribution of the jet pairing in each event with the highest likelihood value is used in the statistical analysis. The distribution for the dominant RunIIb 3-jet channel is shown in the left panel of Figure 2. In the right panel of the same figure good agreement can be seen between the data and background model in a side-band sample selected using an inverted likelihood cut and picking the “wrong” pairing.

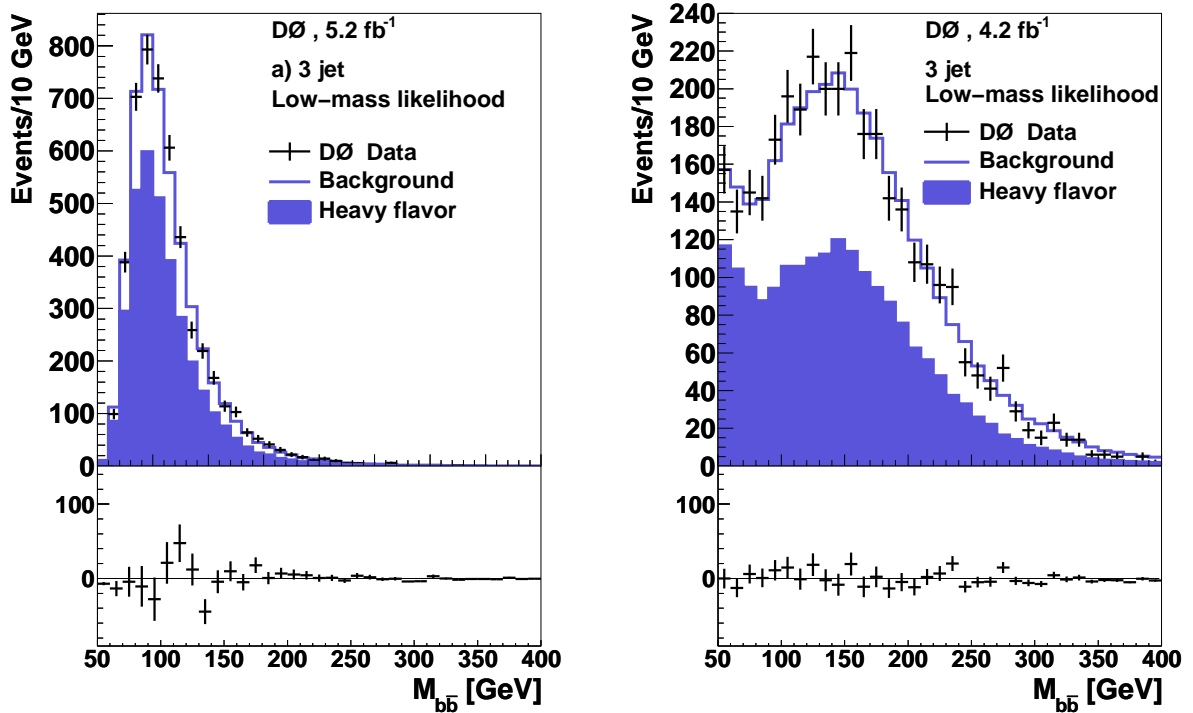


FIG. 2: The dijet invariant mass distribution for the dominant  $bh \rightarrow b\bar{b}$  3-jet channel is shown. In both panels the line shows the background model, the solid histogram the component coming from  $bbb$ , the crosses show the data and the difference between data and the background model is shown below. The normalization of the background is chosen to give the same event yield as observed in the data for the purposes of illustration (this normalization floats in the statistical analysis). The left panel shows the input which is used in evaluating the limits, the right hand panel shows a cross check distribution in a sideband region.

### III. SYSTEMATIC UNCERTAINTIES

Where appropriate, systematic uncertainties are modeled as shape systematics that correlate a varying uncertainty across each bin of the associated input distributions. This contrasts with a flat or rate systematic that introduces a constant uncertainty correlated across each bin of the input distribution - representing an overall uncertainty on the total yield.

In the  $bh \rightarrow b\tau\tau$  analysis for the dominant  $Z$ +jets backgrounds, uncertainties are estimated using  $Z \rightarrow \mu\mu$  control samples:  $Z$ +jets(3.2%) and  $Z + b$ -tagged jets (5%) normalizations, inclusive trigger efficiency (3% - common to all simulated backgrounds) and a shape uncertainty of  $\sim 1\%$  from the modeling of the  $Z$  boson kinematics. For the non- $Z$  boson and non-multi-jet backgrounds there are rate uncertainties: hadronic tau reconstruction efficiency (4-10%), (luminosity (6.1%), muon reconstruction efficiency (2.9%), single muon trigger efficiency (1.3%),  $t\bar{t}$ (11%) and diboson

(8%) production cross sections. Further important sources of uncertainty affecting the shape of the final discriminant distributions comes from the jet energy scale (10%) and  $b$ -tagging efficiency modeling (5%). The uncertainty on the multi-jet background yield varies between 10-40%. With the exception of the hadronic tau reconstruction efficiency and multi-jet normalization, that are evaluated for each tau type separately, these uncertainties are assumed 100% correlated across all tau channels.

In the  $bh \rightarrow bb\bar{b}$  analysis only systematic variations in the shape of the background distribution are considered - the overall background normalization is unconstrained in the profile likelihood and thus allowed to float freely in the fitting procedure (independently for the test and null hypotheses) during evaluation of the limits. The dominant sources of uncertainty in the shape of the background distribution arise from the measurement of the rate at which light partons fake a heavy flavor jet and the  $b$ -tagging efficiency. For the signal model, the  $b$ -tagging efficiency (11-18%) and the jet energy scale (2-10%) dominate the experimental uncertainties.

Most of the experimental uncertainties are uncorrelated between the two contributing analyses with the exceptions being those arising from the  $b$ -quark tagging efficiency and the jet modeling systematics which are assumed 100% correlated between channels.

#### IV. COMBINED RESULTS AND INTERPRETATION WITH THE MSSM

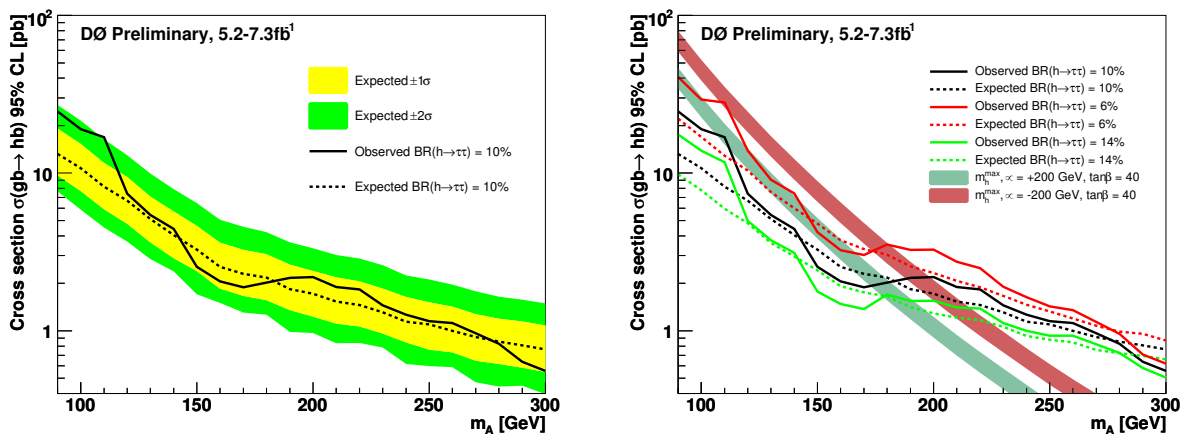


FIG. 3: Combined 95% confidence limits on cross section  $\sigma(gb \rightarrow hb)$  for  $p_T^b > 12$  GeV and  $|\eta^b| < 5.0$ . The left panel shows the limit assuming the tree-level branching fraction  $\text{BR}(h \rightarrow \tau\tau) = 0.1$ , where the black solid line shows the observed limit, the dash line the expected limit and the light and dark shaded bands show the  $\pm 1$  and  $\pm 2$  standard deviations around the expectation. The right panel shows the observed (solid) and expected (dashed) limits for three different assumptions on the branching ratio to tau pairs. The shaded bands show the theoretical prediction, assuming an error of 15% [4], for the cross section for the  $m_h^{\text{max}}$  scenario for two different assumptions for the value of  $\mu$  for  $\tan\beta = 40$ . These give predictions for the tau pair branching fraction that are approximately equivalent to that assumed in the experimental limits.

Limits are set using the *modified frequentist* (or  $CL_s$ ) technique [27]. The test statistic is a negative log-ratio of profiled likelihoods [28]:

$$LLR = -2 \ln \frac{p(\text{data}|H_1)}{p(\text{data}|H_0)}, \quad (1)$$

where  $H_1$  is the test (background + signal) hypothesis,  $H_0$  is the null (background only) hypothesis and  $p$  are the profile likelihoods based on Poisson probabilities for obtaining the observed number of events under each hypothesis.  $CL_s$  is defined by the ratio:  $CL_s = CL_{s+b}/CL_b$  where,  $CL_{s+b}$  and  $CL_b$  are the  $p$ -values for the test and null hypothesis respectively. These  $p$ -values are estimated from the integrals of the respective sampling distributions generated using Monte Carlo simulated pseudo-data.

For the individual contributing analyses exclusion limits have been set both within the framework of the MSSM and in a roughly model independent way on the cross-section  $\times$  branching ratio. This later approach is not generally

applicable when combining channels with different production modes or final states since the relative signal yields in each contributing channel typically will depend on the particular model scenario being considered. For this combination, since the two channels share a production mode, and the Higgs width is largely narrower than the experimental resolution for much of the interesting model space, it is possible to construct an exclusion region which is somewhat less model dependent than the typical MSSM exclusion analyses. The only additional model assumptions with respect to the “model independent” procedures used in the contributing analyses is that the Higgs boson decays only to tau and  $b$ -quark pairs. The 95% confidence limit on the production cross section  $\sigma(gb \rightarrow hb)$  with respect to the acceptance cuts on the spectator  $b$ -quark are shown in Figure 3 for three different choices for the branching fraction to tau pairs,  $\text{BR} = 6\%$ ,  $10\%$  and  $14\%$ . The  $bh \rightarrow b\tau\tau$  channel tends to dominate the limit up to around  $M_A = 180$  GeV. The increasingly important contribution from the  $bh \rightarrow bb\bar{b}$  channels as the mass increases is responsible for the visible decrease in the dependence of the limit on the tau branching fraction.

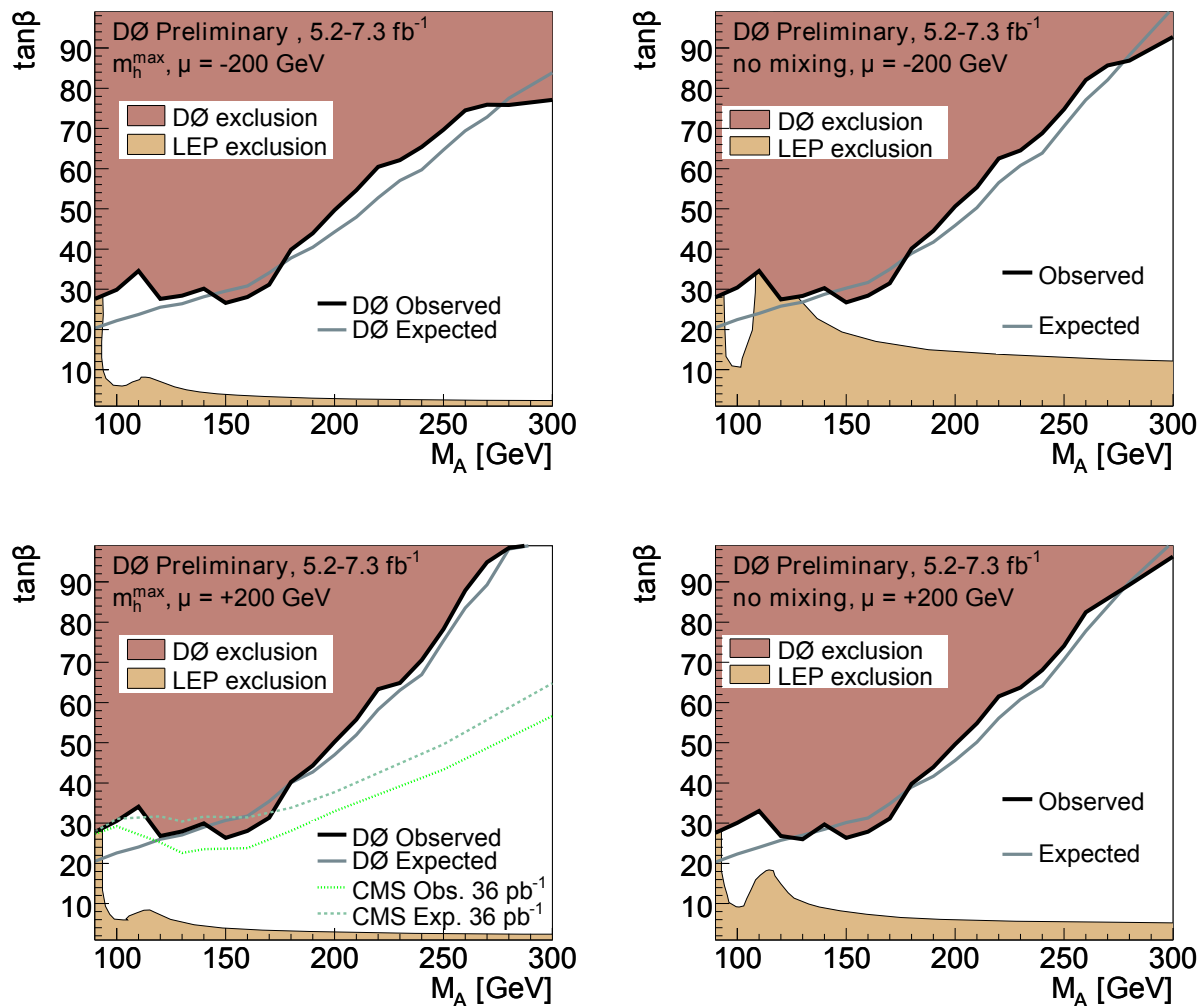


FIG. 4: 95% Confidence limits in the  $\tan\beta$ - $M_A$  plane for 2 benchmark scenarios:  $m_h^{\max}$  (left) and no-mixing (right) for  $\mu < 0$  (top) and  $\mu > 0$  (bottom). The black line shows the observed limit, the grey line the expected limit. The dark shaded regions demonstrates the observed exclusion and the light shaded region that from LEP. The latest published results from CMS [16] are also shown for the  $m_h^{\max}$ ,  $\mu > 0$  scenario (bottom left).

Limits have been set within four MSSM scenarios [29] in the  $M_A - \tan\beta$  plane and are shown in Figure 4. In addition to the experimental uncertainties an additional 15% theoretical uncertainty on the production cross section is included with contributions from scale variations and PDF uncertainties. The four scenarios considered are defined in terms of:  $M_{SUSY}$ , the mass scale of squarks,  $\mu$ , the Higgs sector bilinear coupling,  $M_2$ , the gaugino mass term,  $X_t$ , the mixing parameter,  $A_t$ , the trilinear coupling of the stop sector,  $A_b$ , the trilinear coupling of the sbottom sector

and  $m_{\tilde{g}}$  the gluino mass term. The maximal-mixing,  $m_h^{max}$ , scenario is defined as:

$$\begin{aligned} M_{\text{SUSY}} &= 1\text{TeV}, \mu = 200\text{GeV}, M_2 = 200\text{GeV}, \\ X_t &= 2M_{\text{SUSY}} \\ A_b &= A_t, m_{\tilde{g}} = 0.8M_{\text{SUSY}}. \end{aligned}$$

and the no-mixing scenario - with vanishing mixing in the stop sector and a higher SUSY mass scale to avoid the LEP Higgs bounds:

$$\begin{aligned} M_{\text{SUSY}} &= 2\text{TeV}, \mu = 200\text{GeV}, M_2 = 200\text{GeV}, \\ X_t &= 0, A_b = A_t, m_{\tilde{g}} = 0.8M_{\text{SUSY}}. \end{aligned}$$

Four scenarios are constructed from these two by the consideration of both + and - signs for  $\mu$ .

The SM cross section  $gb \rightarrow hb$  is taken from MCFM and then corrected to the appropriate  $\sigma \times \text{BR}$  using couplings and branching fractions taken from FEYNHIGGS [30] (see also [31]). For larger values of  $\tan\beta$  the width of the Higgs can become comparable to the experimental resolution - in particular for the  $h \rightarrow b\bar{b}$  final state. This is taken into account using the method described in [4].

These results exclude a wide region of the MSSM parameter space and represent the strongest limits to-date from the Tevatron.

### Acknowledgments

We thank the staffs at Fermilab and collaborating institutions, and acknowledge support from the DOE and NSF (USA); CEA and CNRS/IN2P3 (France); FASI, Rosatom and RFBR (Russia); CNPq, FAPERJ, FAPESP and FUNDUNESP (Brazil); DAE and DST (India); Colciencias (Colombia); CONACyT (Mexico); KRF and KOSEF (Korea); CONICET and UBACyT (Argentina); FOM (The Netherlands); STFC and the Royal Society (United Kingdom); MSMT and GACR (Czech Republic); CRC Program and NSERC (Canada); BMBF and DFG (Germany); SFI (Ireland); The Swedish Research Council (Sweden); and CAS and CNSF (China).

- 
- [1] H.P. Nilles, Phys. Rep. **110**, 1 (1984); H.E. Haber and G.L. Kane, Phys. Rep. **117**, 75 (1985).
  - [2] S. Schael *et al.* (The ALEPH, DELPHI, L3, and OPAL Collaborations), Eur. Phys. J. C **47**, 547 (2006).
  - [3] V.M. Abazov *et al.* (D0 Collaboration), Nucl. Instrum. Methods Phys. Res. A **565**, 463 (2006).
  - [4] V.M. Abazov *et al.* (D0 Collaboration), Phys. Lett. B **698**, 97 (2011).
  - [5] V.M. Abazov *et al.* (D0 Collaboration), arXiv:1106.4885, submitted to Phys.Rev.Lett.
  - [6] V.M. Abazov *et al.* (D0 Collaboration), Phys. Rev. Lett. **95**, 151801 (2005).
  - [7] V.M. Abazov *et al.* (D0 Collaboration), Phys. Rev. Lett. **97**, 121802 (2006).
  - [8] V.M. Abazov *et al.* (D0 Collaboration), Phys. Rev. Lett. **101**, 071804 (2008).
  - [9] V.M. Abazov *et al.* (D0 Collaboration), Phys. Rev. Lett. **101**, 221802 (2008).
  - [10] V.M. Abazov *et al.* (D0 Collaboration), Phys. Rev. Lett. **102**, 051804 (2009).
  - [11] V.N. Abazov *et al.* (D0 Collaboration), Phys. Rev. Lett. **104**, 151801 (2010).
  - [12] V.M. Abazov *et al.* (D0 Collaboration), arXiv:1106.4555, submitted to Phys.Lett.B.
  - [13] A. Abulencia *et al.* (CDF Collaboration), Phys. Rev. Lett. **96**, 011802 (2006).
  - [14] T. Aaltonen *et al.* (CDF Collaboration), Phys. Rev. Lett. **103**, 201801 (2009).
  - [15] T. Aaltonen *et al.* (CDF Collaboration), arXiv: 1106.4782, submitted to Phys.Rev.D.
  - [16] S. Chatrchyan *et al.* (CMS Collaboration), arXiv: 1104.1619, submitted to Phys.Rev.Lett.
  - [17] G. Blazey *et al.*, arXiv:hep-ex/0005012 (2000).
  - [18] V.M. Abazov *et al.* (D0 Collaboration), Phys. Rev. Lett. **101**, 062001 (2008).
  - [19] V.M. Abazov *et al.* (D0 Collaboration), Nucl. Instrum. Methods Phys. Res. A **620**, 490 (2010).
  - [20] T. Sjöstrand *et al.*, arXiv:hep-ph/0308153 (2003).
  - [21] J. Campbell, R.K. Ellis, F. Maltoni, and S. Willenbrock, Phys. Rev. D **67**, 095002 (2003).
  - [22] S. Jadech *et al.*, Comput. Phys. Commun. **76** (1993) 361
  - [23] E. Boos *et al.* (CompHEP Collaboration), Nucl. Instrum. Meth. A **534** (2004) 250.
  - [24] R. Brun and F. Carminati, CERN program library long writeup W5013 (1993). GEANT3 was used.
  - [25]  $\eta_{\text{det}}$  is the pseudorapidity defined with respect to a vertex of (0,0,0) and is a particularly useful measure for defining acceptance cuts which need to be aligned with detector boundaries.

- [26] M.L. Mangano *et al.*, JHEP 07, 001 (2003).
- [27] T. Junk, Nucl. Instrum. Meth. A **434** (1999) 435.; R. Barate *et al.*, Phys. Lett B **565** (2003).
- [28] W. Fisher, FERMILAB-TM-2386-E (2007).
- [29] M. Carena, S. Heinemeyer, C. E. M. Wagner, and G. Weiglein, Eur. Phys. J. C **45**, 797 (2006).
- [30] S. Heinemeyer, W. Hollik, and G. Weiglein, Eur. Phys. J. C **9**, 343 (1999); Comput. Phys. Commun. **124**, 76 (2000); G. Degrassi *et al.*, Eur. Phys. J. C **28**, 133 (2003), M. Frank *et al.*, JHEP **0702**, 047 (2007). FEYNHIGGS version 2.8.1
- [31] D. Noth, M. Spira, Phys. Rev Lett **101**, 181801 (2008), L. Hofer, U. Nierste, D. Scherer, JHEP **10**, 081 (2009).